Tellurium: A new active element for innovative multifunctional bioactive glasses

Tellurium: a new active element for innovative multifunctional bioactive glasses

Marta Miola[1,2,*], Jonathan Massera[3], Andrea Cochis[4,5], Ajay Kumar[4,5], Lia Rimondini[4,5], Enrica Vernè[1,2]

[1] Department of Applied Science and Technology, Politecnico di Torino, corso Duca degli Abruzzi 24, 10129 Torino (TO), Italy

[2] Polito[Bio]MED Lab, Politecnico di Torino, Politecnico di Torino, Via Piercarlo Boggio 59, 10138 Torino (TO), Italy

[3] Faculty of Medicine and Health Technology, Laboratory of Biomaterials and Tissue Engineering, Tampere University, Korkeakoulunkatu 3, 33720 Tampere, Finland.

[4] Department of Health Sciences, Università del Piemonte Orientale UPO, Via Solaroli 17, 28100 Novara (NO), Italy

[5] Interdisciplinary Research Center of Autoimmune Diseases, Center for Translational Research on Autoimmune and Allergic Diseases-CAAD, Corso Trieste 15A, 28100 Novara (NO), Italy

* Corresponding author

Dr. Marta Miola
Politecnico di Torino
Department of Applied Science and Technology, Politecnico di Torino, Torino (TO), Italy
Institute of Materials Engineering and Physics
Corso Duca degli Abruzzi, 24 - 10129 (TORINO) ITALY
Tel: +39 0110904717
Fax: +39 011 0904624

Abstract

Bioactive glasses have been widely investigated for their ability to release ions with therapeutic effect. In this paper, a silica-based-bioactive glass was doped with a low-amount of tellurium dioxide (1 and 5 mol%) to confer antibacterial and antioxidant properties. The obtained glasses were characterized in terms of morphology, composition, structure, characteristic temperatures and *in vitro* bioactivity. Moreover, comprehensive analyses were carried out to estimate the cytocompatibility, the antibacterial and antioxidant properties of Te-doped glasses. The performed characterizations evidenced that the Te insertion did not interfere with the amorphous nature of the glass, the substitution of SiO_2 with TeO_2 lead to a slight decrease in T_g and a TeO_2 amount higher than 1 mol% can induce a change in the primary crystal field. *In vitro* bioactivity test demonstrated the Te-doped glass ability to induce the precipitation of hydroxyapatite. Finally, the biological characterization evidenced a strong antibacterial and antioxidant effects of Te-containing glasses in comparison with control glass, demonstrating that Te is a promising element to enhance the biological response of biomaterials.

Keywords

Tellurium; Bioactive glasses; Antibacterial; Antioxidant; Cytocompatibility.

1. Introduction

Bioactive glasses, discovered by professor Larry Hench fifty years ago, have been widely investigated for their role in bone tissue regeneration, since they can chemically bond to living bone through a well-known process, which involves a rapid ion-exchange between glass surface and surrounding biological fluids, leading to the

formation of biologically active hydroxyapatite (HAp) [1, 2]. Recently, the role of bioactive glasses in the soft tissue regeneration has been also explored [3-5] and it has been demonstrated that the controlled release of specific ions can stimulate several processes that regulate the regeneration of hard and soft tissues. For example Si, Ca, P and Mg plays a fundamental role in the formation and calcification of bone tissue, also Sr shows to stimulate bone formation and to reduce the bone resorption. Other elements, such as Cu and Co stimulate the proliferation of human endothelial cells and enhance the angiogenesis processes. Finally, different element, such as Ag, Cu, Zn, and Ga possess antimicrobial/anti-inflammatory properties

In the last years, many effort have been made to improve the biological activity of bioactive glasses, by the incorporation in the glasses formulation of tailored amount of active elements, such as Sr, Cu, Ag, Zn, Mn, etc… [6-12]. In this prospective, the efforts of the researchers have been addressed to design new bioactive glass compositions by doping both silica and phosphate-based glasses with therapeutic ions and investigating the effect of their release on cell viability and on gene stimulation towards regeneration and self-repair path (i.e. the genetic design of bioactive glasses [13-17]).
Among the functionalities that can be imparted by active ions, the antimicrobial properties are the most investigated [7-9, 18-20]; moreover, the antioxidant effect of some bioactive glass formulations have been also explored [21]. The increasing growth of micro-organisms resistance to antibiotics [22] leads the researchers to inspect the antimicrobial role of different agents and develop innovative materials able to reduce the adhesion and proliferation of bacteria, and thus limiting the infection development. Bioactive glasses compositions containing antibacterial element, such as Ag, Cu, Zn and Ga, have been deeply examined [7-9, 18-20] and their ability to limit the bacterial growth was confirmed also towards antibiotic-resistant strains. However, recently, the ability of bacteria to develop resistance towards also metallic ions, such as silver ions, was observed [23, 24]; for this reason, there is a continuous need to create new solutions for infection control and to find new antimicrobial agents.

Among the poorly explored elements with potentially antibacterial and antioxidant properties, tellurium has attracted our attention since, although it is considered a non-essential trace element and it shows a dose-related and chemical form-related toxicity, its important biological effects have been recently investigated [25-27].

Tellurium is an element belonging to the chalcogens group showing different oxidation state that has been barely considered in biology and biochemistry. However, some studies demonstrated that Te, and its compounds, can be used as biomarkers, as well as possess antimicrobial, antioxidant and antitumoral effect [25]. In particular, Cailing et al. [26] demonstrated that tellurium dioxide nanoparticles (TeO_2 NPs) have strong antioxidant activity and antimicrobial effect against some Gram negative (*Escherichia coli, Salmonella enteritidis*) and Gram positive (*Bacillus subtilis*) bacteria. Recently, another study [27] investigated the antimicrobial and antioxidant activity of tellurium nanorods biologically synthesized by *Pseudomonas pseudoalcaligenes* in comparison to K_2TeO_3. This study evidenced a higher antioxidant effect of Te nanorods than K_2TeO_3; on the contrary, the antibacterial and antifungal activity of nanorods was significantly lower than K_2TeO_3. However, authors affirmed that further investigations are required to investigate the mechanism of action of biosynthesized Te nanorods.

Besides, very few studies concerned the development of Te-doped biomaterials. Ma et al. [28] synthesized a tellurium/calcium silicate nanocomposite composed by tellurium nanorods dispersed in the calcium silicate matrix. This composite evidenced good biocompatibility at low nanorods concentration (10-20 μg/ml,) towards human gastric carcinoma cells (MGC-803); nevertheless, the authors did not investigate the potential antimicrobial and/or antioxidant effect of Te-containing composite. Moreover, on the basis of author's knowledge, there is only one study concerning the development of a bioactive glass containing tellurium [29]. Damrawi et al. [29] synthesized tellurite glasses/glass ceramics, by completely substituting silica with TeO_2, and studied this composition from the viewpoint of bioactivity. They evidenced the Te-based glasses/glass ceramics ability to induce the nucleation of hydroxyapatite and thus the possibility to be used

as bioactive implant. However, this study did not evaluate the possible toxic effects of the Te-based material and did not investigate their possible efficacy in terms of antimicrobial and antioxidant effect.

In this paper, we evaluate for the first time the possibility to develop innovative silica-based bioactive glasses containing a low-amount of tellurium dioxide, in order to impart both antibacterial and antioxidant properties, maintaining contemporaneously the cytocompatibility. For this reason, we doped a bioactive glass composition with 1 and 5 mol% of TeO_2, by substituting SiO_2 with TeO_2, and we characterized the obtained samples in terms of, morphology, composition, structure, reactivity in simulated physiological fluids and biological response (cytocompatibility, antioxidant and antibacterial effect).

2. Materials and Methods

2.1 Glasses synthesis

Three glass compositions (STe0, STe1 and STe5), reported in table 1, were developed by partially substituting SiO_2 with TeO_2. The glasses were synthesized by melt and quenching process: the reactants (purchased from Sigma Aldrich) were placed in a Pt crucible and melted at 1450 °C for 1 hour; the melt was poured both in water, obtaining a frit, and on a brass mold to realize glass bars that were annealed at 550 °C for 14 hours. The frit was subsequently milled in a ZrO_2 6-ball planetary mill (Fritsh, Pulverisette 6) and sieved to obtain powders < 25 μm; the bars were cut in slice of about 10x10x1 mm by means of an automatic cutter (ATA, Brillant 220), that were polished with abrasive SiC papers (up to 1000 grit).

Table 1: nominal composition of investigated glasses.

	%mol		
	STe0	**STe1**	**STe5**
SiO_2	48.6	47.6	43.6
Na_2O	16.7	16.7	16.7
CaO	34.2	34.2	34.2
P_2O_5	0.5	0.5	0.5
TeO_2	0.0	1.0	5.0

2.2 Glasses characterizations

Morphological and compositional analyses of glasses were performed using a Field Emission Scanning Electron Microscopy (FESEM, SUPRATM 40, Zeiss) equipped with X-ray energy dispersive spectroscopy (EDS). For FESEM observation the glass powders were coated with a Cr layer.

To assess the amorphousness or extent of crystallization, X-ray diffraction analysis (XRD) was carried out by means of a X'Pert diffractometer (voltage 40 kV and current 30 mA) using a Bragg-Brentano camera geometry with Cu Kα incident radiation, incident wavelength λ = 1.5405 Å, step size Δ(2θ) = 0.02° and fixed counting time of 1 s per step. The obtained spectra were analyzed by X'Pert HighScore program equipped with PCPDFWIN database.

Fourier transformation infrared spectroscopy (FT-IR SpectrumOne, Perkin Elmer) was used to verify the structure of the synthesized glasses. FT-IR spectra were acquired in the 600 - 4000 cm^{-1} with a resolution of 1 cm^{-1}. All spectra were background corrected and normalized to the peak with higher intensity.

Glass powders were subjected to SDTA (STA 449 F1 Jupiter, Netzsch Group, Selb, Germany) analysis in air atmosphere to evidence possible effects of Te introduction on glass characteristic temperatures, i.e. glass

transition temperature (T_g), peak crystallization temperature (T_c) and melting temperature (T_m). The analysis was recorded using a heating rate of 10°C/min on glass powders < 25 μm.

2.3 In vitro bioactivity test

The bioactivity of the three glasses was investigated both in simulated body fluid (SBF), following Kokubo protocols [30] and in TRIS (pH 7.4) [31] in order to evaluate the effect both of the soaking solution and of the glass composition on the reactivity. Specifically, according to a the study reported by the Technical Committee 4 (TC04) of the International Commission on Glass (ICG) [32], 150 mg of glass powders were immersed in 100 ml of SBF or TRIS, the solutions were stirred at 100 rpm at 37 °C in orbital shaker (IKA KS4000i control) up to 14 days. The pH of the solutions was measured after every 2/3 days and the test was performed in triplicate.

After immersion, glasses were gently washed with bi-distilled water, dried at room temperature and analyzed by means of XRD, FT-IR and Raman. The Raman spectra were recorded using a 532 nm wavelength laser (Cobolt Samba) and measured with a 300 mm spectrograph (Andor Shamrock 303) and acooled CCD camera for data collection (Andor Newton 940P). All spectra were recorded over the 2000 cm^{-1} - 100 cm^{-1} range and normalized to the band showing the maximum intensity. *Biological characterizations*

2.4 Biological characterizations

Biological characterizations were performed on square specimens (10x10x1 mm). Specimens were heat-sterilized for 3 hours at 100°C and stored at room temperature protected from light prior to biological experiments.

2.4.1 Cytocompatibility evaluation

Human bone marrow- derived stem cells (hBMSCs) were kindly provided by Prof. P. Genever, University of York. They were isolated from bone marrow, immortalized through hTERT lentiviral vectors (hBMSCs Y201) and used for *in vitro* experiments [33]. Cells were cultivated in low-glucose Dulbecco's modified Eagle Medium (DMEM, Sigma-Aldrich) supplemented with 15% fetal bovine serum (FBS, Sigma) and 1% antibiotics (penicillin/streptomycin) at 37 °C, 5% CO_2 atmosphere. Cells were cultivated until 80-90% confluence, detached by trypsin-EDTA solution, harvested and used for experiments.

2.4.2 Metabolic evaluation

Cells were directly seeded onto specimens' surface at constant concentration ($3x10^4$ cells/specimen) and cultivated for 1, 2 and 3 days. At each time points, the viability of the cells in direct contact with specimens were evaluated by means of the metabolic colorimetric Alamar blue assay (alamarBlue™, from Life Technologies) following Manufacturer's instructions. Briefly, supernatants were removed from each well containing cells and replaced with Alamar blue solution (10% v/v in fresh medium). Plates were incubated in the dark for 4 h and then 100 μl were removed, spotted into a new black 96-well plate and fluorescence signals were evaluated with a spectrophotometer (Spark®, Tecan Trading AG, CH) using the following set-up: fluorescence excitation wavelength 570 nm, fluorescence emission reading 590 nm.

2.4.3 ROS/RNS scavenge

Cells were seeded onto specimens' surface as prior described for the metabolic evaluation. At 1, 2 and 3 days, cells were treated with 300 μM H_2O_2 for 3 hours/day to test tellurium antioxidant activity to scavenge the derived ROS and RNS species [34]. Cells metabolism were checked by the Alamar blue to compare values pre- and after-H_2O_2 treatment. The active species quantification was performed with the fluorescent OxiSelect™ assay (from Cell Biolabs) following Manufactures' instructions. Briefly, 50 μl of the test specimens' supernatants were collected and mixed with 50 μl of catalyst and 100 μl of the DCFH solution (both provided from the kit); after 45 minutes incubation the fluorescence signal was evaluated by spectrophotometer (Spark®, Tecan Trading AG, CH) using the following set-up: fluorescence excitation wavelength 480 nm,

fluorescence emission reading 530 nm. Cells cultivated onto bioactive glasses without H_2O_2 stress were considered as control.

2.4.4 Osteogenesis

Cells were directly seeded onto specimens' surface at constant concentration ($2x10^4$ cells/specimen) and cultivated for 7, 14 and 21 days in the presence of osteogenic medium (low-glucose DMEM supplemented with 10% FBS, 10^{-7} M dexamethasone, 50 μM β-glycerophosphate, 20 mM ascorbic acid). Cells were stressed with 300 mM H_2O_2 for 3 hours/day as prior described; then, at each time-point the supernatants were collected and the alkaline phosphatase (ALP) activity was measured to evaluate osteogenesis progression in the presence of inflammation. ALP activity was evaluated by a colorimetric assay (ab83369, from AbCam, UK) following Manufacturer's instructions: briefly, 80 μl of supernatants were collected from each sample and mixed with 50 μl of the pNPP solution and 10 μl of the ALP enzyme. After 60 minutes incubation, the reaction was stopped and the optical density was measured by spectrophotometer (Spark®, Tecan Trading AG, CH) using a 405 nm wavelength.

After 21 days of culturing, the formation of calcium deposit was evaluated by the alizarin red staining. Briefly, cells were fixed (4% formaldehyde, 15 minutes) and then incubated 30 minutes with the alizarin solution (from Sigma, 40 mM in PBS). Afterwards, deposited alizarin was solved with 10% acetic acid (5 minutes), collected and centrifuged to separate the pellet (20000 g, 15 min). Supernatants optical density was evaluated by a spectrophotometer (Spark®, Tecan Trading AG, CH) at 490 nm wavelength.

2.4.5 Antibacterial activity

Strains growth conditions

To test antibacterial activity of the tellurium doped glasses, the orthopedic-related strains *Staphylococcus aureus* (*S. aureus*) and Staphylococcus epidermidis (*S. epidermidis*) were used. *S. aureus* was purchased from the American Type Culture Collection (ATCC, 43300) while *S. epidermidis* was clinically isolated from the Clinical Microbiology Unit of the Maggiore Hospital of Novara. Bacteria were cultivated onto Trypticase Soy Agar (TSA, Sigma-Aldrich) and incubated at 37 °C until round single colonies were formed; then, 2-3 colonies were collected and spotted into 30 ml of Luria Bertani broth (LB, Sigma-Aldrich). Broth cultures were incubated overnight at 37 °C in agitation (120 rpm in an orbital shaker), then bacteria concentration was adjusted to $1x10^5$ cells/ml by diluting in fresh media until optical density of 0.001 at 600 nm was reached as determined by spectrophotometer (Spark®, Tecan Trading AG, CH).

Biofilm formation

Sterile specimens were gently placed into a 24 multiwell plate by sterile tweezers avoiding any surface damages. Each specimen was submerged with 1 ml of the $1x10^5$ cells/ml broth bacteria culture prepared as prior described; plate was incubated for 90 minutes in agitation (120 rpm) at 37 °C to allows the separation between adherent biofilm cells and not-adherent floating planktonic cells (separation phase) [35, 36]. Afterwards, supernatants containing planktonic cells were removed and replaced with 1 ml of fresh media to cultivate surface-adhered biofilm cells (growth phase). Biofilm were grown at 37 °C for 1, 2 and 3 days prior to evaluations.

Biofilm Metabolic evaluation

At each time-point, specimens were gently washed 3 times with PBS to remove non-adherent cells and then moved to a new 24 multiwell plate where bacteria metabolic activity was evaluated by the Alamar blue assay as prior described for cells metabolic activity evaluation.

2.4.6 Co-cultures

Specimens' ability to preserve cells from infection was evaluated by a cells-bacteria co-culture assay as prior described by the Authors [37ref]. A defined number ($3x10^4$ cells/specimen) of BMSCs were seeded onto specimens' surface and allowed to adhere and spread for 24 hours at 37 °C. The day after, medium was removed, and specimens were infected with 1 ml of antibiotics-free DMEM containing $1x10^5$ bacteria (*S. aureus* or *S. epidermidis*). After 24 hours infection, specimens were collected and surface adhered cells and bacteria were detached by trypsin digestion (10 min at 37 °C); cells were marked by trypan blue and counted

by a Burker chamber to determine viable number, while bacteria were diluted by 6-ten-fold dilutions step and numbered by the CFUs count, as prior described [38].

2.5 Statistical Analysis of Data

Experiments were performed using 6 replicates. Results were statistically compared by the SPSS software (v25, IBM) using the one-way ANOVA test and the Tukey's post-hoc analysis. Results were considered as significant for $p<0.05$.

3. Results and Discussion

3.1 Glasses characterization

Figure 1 shows the morphological and compositional analysis performed with FESEM-EDS. Glass powders have the typical sharp-cornered morphology of ball-milled glass and, as expected, a grain size < 25 µm. EDS analysis (Figure 1d-f) showed the presence of all elements characteristic of the glasses, in particular the Te peaks for STe1 and STe5 glasses, confirming the effective Te introduction.

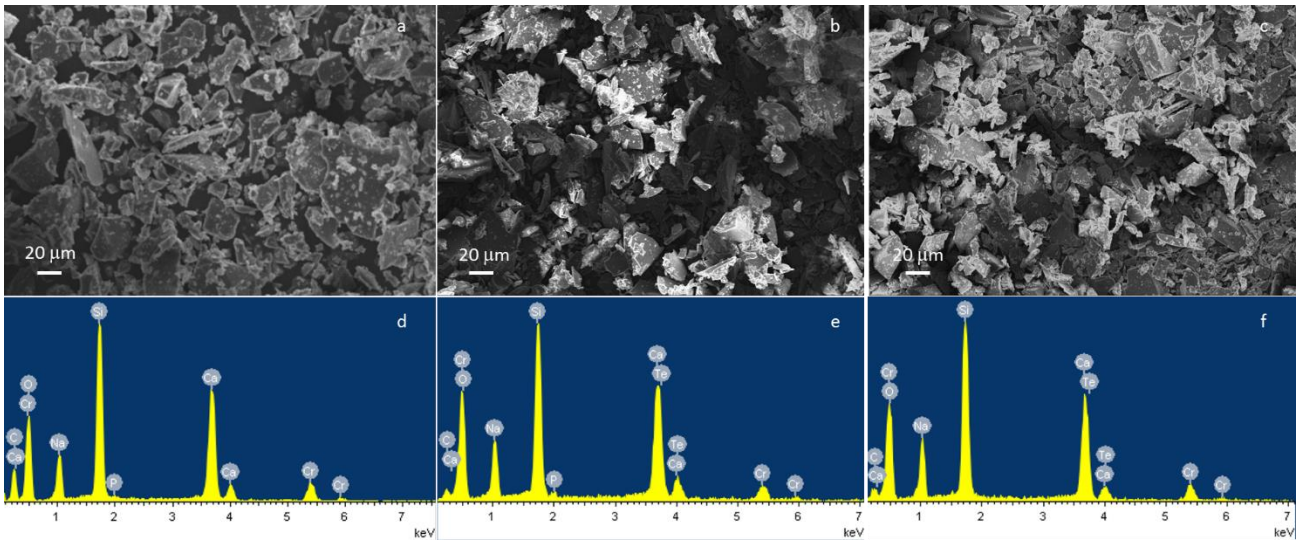

Figure 1: FESEM-EDS analysis of STe0 (a,d), STe1 (b,e) and STe5 (c,f) powders < 25 µm.

Figure 2 shows the structural characterization of the three glasses. The XRD analysis confirms the amorphous nature of the materials, since, as it can be observed, all spectra showed the typical amorphous halo between 2 Theta 25°-35° and no crystallization peak is evident. Thus, the Te insertion do not induce the nucleation of crystalline phases.

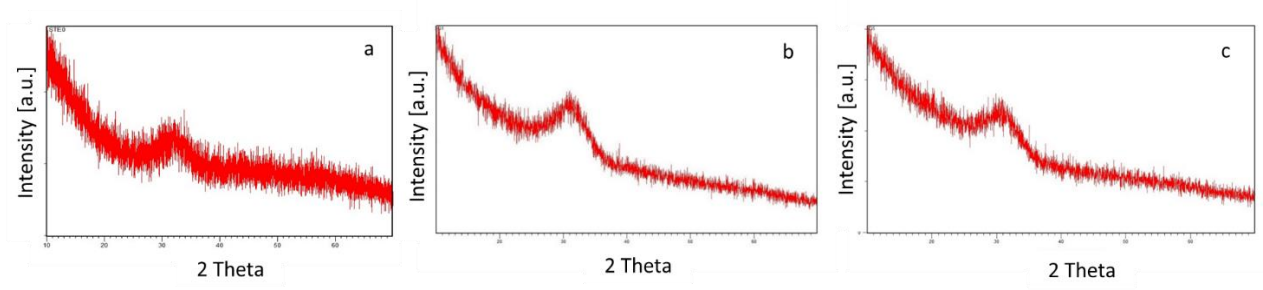

Figure 2: XRD analysis of STe0, STe1 and STe5 powders < 25 µm.

FT-IR spectra of the three glasses of investigation are reported in figure 3. For all glasses a band at about 850 cm^{-1} can be attributed to symmetric bending bond of Si-O-Si; the band at 900 cm^{-1} can be assigned to Si-O-Si stretching with non-bridging oxygen (SiO_{NBO}) and the band at 1010 cm^{-1} to the asymmetric stretching mode of Si-O-Si [39-41]. Regarding STe0 glass, an additional band centered at about 1460 cm^{-1} was evidenced, this band can be assigned to the $\nu_3(CO_3^{2-})$ due to the adsorption of carbonates on glass surface [40, 42]. Moreover, the spectra of Te-doped glasses, especially STe5 glass, evidenced a broad peak at 700 cm^{-1} associated with the Te-O-Te vibration mode [43-45].

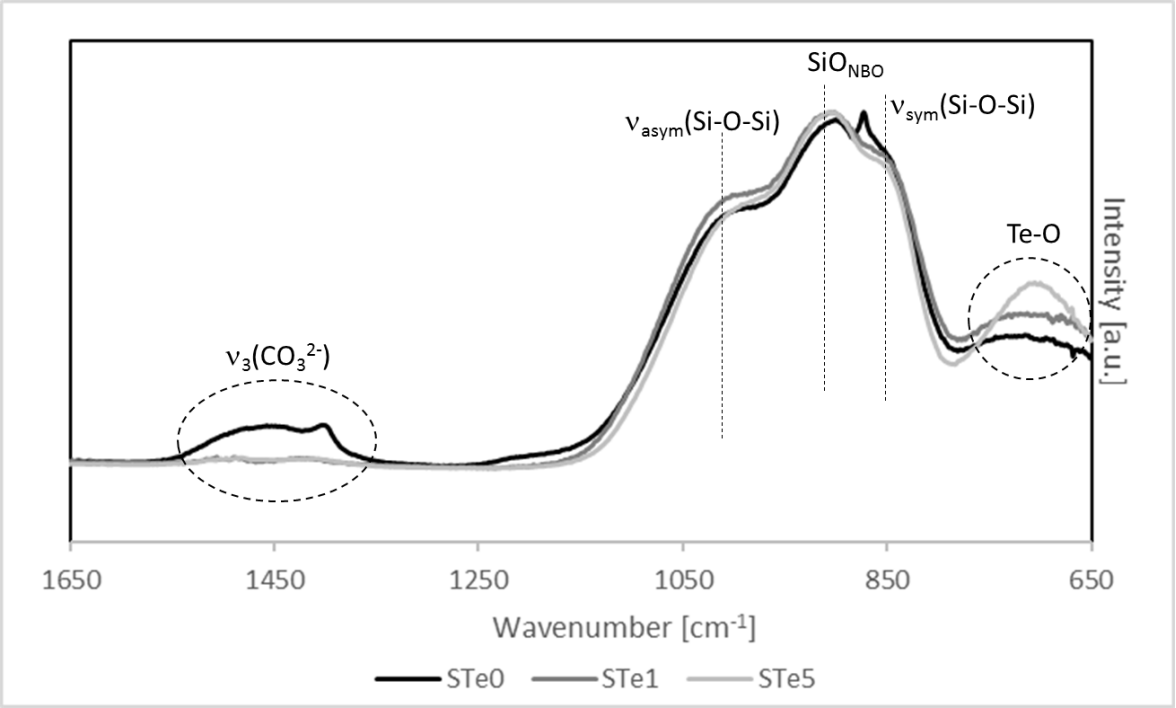

Figure 3: FT-IR spectra of STe0, STe1 and STe5 powders < 25 μm.

Figure 4 shows the DTA spectra of the glasses of investigation. All spectra show a clear glass transition, crystallization and melting. The crystallization and melting present a main peak and a shoulder, indicating crystallization of at least two crystal phases. Table 2 reports the obtained glass transition temperatures (T_g), peak crystallization temperatures (T_c) and melting temperatures (T_m). As it can be noticed, substitution of Si with Te leads to a monotonic decrease in T_g, as already reported in the $0.30Li_2O$-0.70 ($xTeO_2$-(1-x)SiO_2) [46]. The change in the crystallization peak is not as straight forward as the T_g. Indeed, while for STe0 and STe1 the shoulder is located at the left of the main crystallization peak, it is located at the right in the spectrum of STe5. Such change in the crystallization peak can reveal a change in the primary crystal field for TeO_2 content above 1 mol%. This is further confirmed by the decrease in the melting temperature for the glass STe5.

[°C]	STe0	STe1	STe5
T_g (±2°C)	611	575	567
T_{c1} (±2°C)	678	695	674
T_{c2} (±2°C)	727	724	671
T_{m1} (±2°C)	1280	1279	1257
T_{m2} (±2°C)	1286	1288	1263

Table 2: Glass transition temperature (Tg), peak crystallization temperature (Tc) and melting temperature (Tm) obtained by DTA analysis.

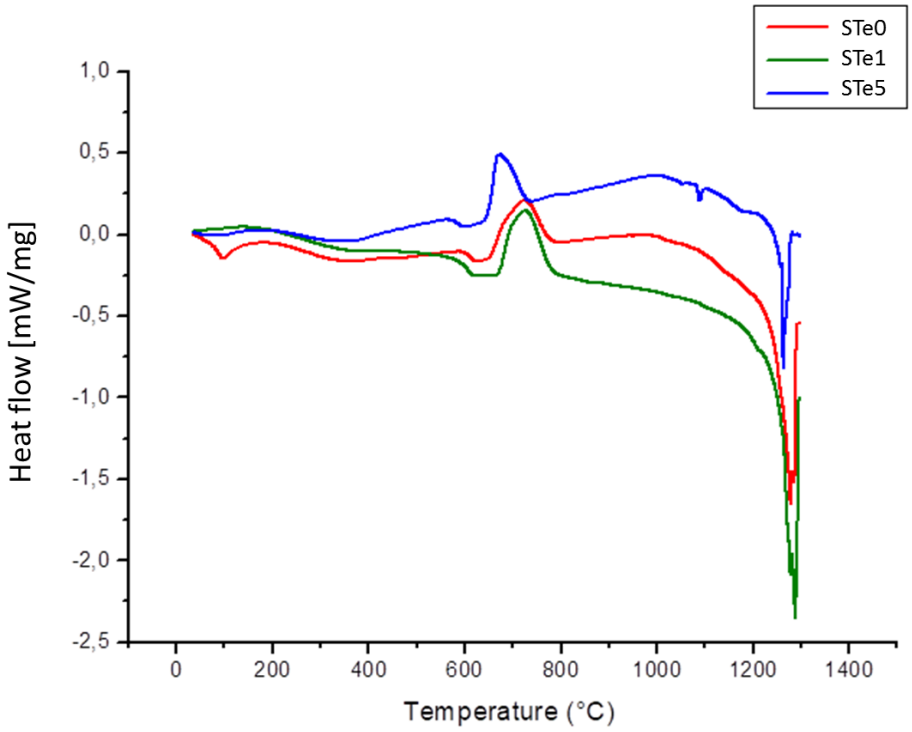

Figure 4: DTA spectra of STe0, STe1 and STe5.

3.2 In vitro bioactivity test

After soaking in SBF and TRIS solution, samples were investigated by means of XRD analysis to evaluate the nucleation of crystalline HAp. Figure 5a-c shows the XRD spectra of glass powders after soaking in SBF solution for 3, 7 and 14 days. After 3 days in SBF, the silica gel halo is well visible between 2 theta 20°-30° in all spectra; moreover, the main peak of HAp (reference code 00-001-1008) is detectable for STe0 and STe1 glasses. The spectra of STe0 evidenced also the presence of calcite (reference code 00-029-0305).

After 7 and 14 days in SBF, the HAp peaks are well visible in all spectra, together with the peaks of calcite for STe0. This analysis evidenced that the Te-doped glasses are able to induce the *in vitro* precipitation of HAp on their surface and thus to promote *in vivo* a chemical bond with bone tissue. Only a slight delay in HAp formation was detected for STe5.

The XRD patterns of the glasses after soaking in TRIS solution are reported in Figure 5d-f. The analysis confirms a slight delay in HAp nucleation for glass containing Te, especially for STe5. As it can be observed, after 3 days of treatment a silica gel halo is well visible for all samples, while the main peak of HAp was observed only on STe0 pattern (Figure 5c). After 14 days, the characteristic peaks of HAp at about 2 theta = 32° can be observed for all samples. As expected, the HAp precipitation rate in TRIS buffer was slower than in SBF solution, since TRIS does not provide the ions useful for the HAp formation, which likely results by the rearrangement of calcium and phosphate species released from the glass surface [47].

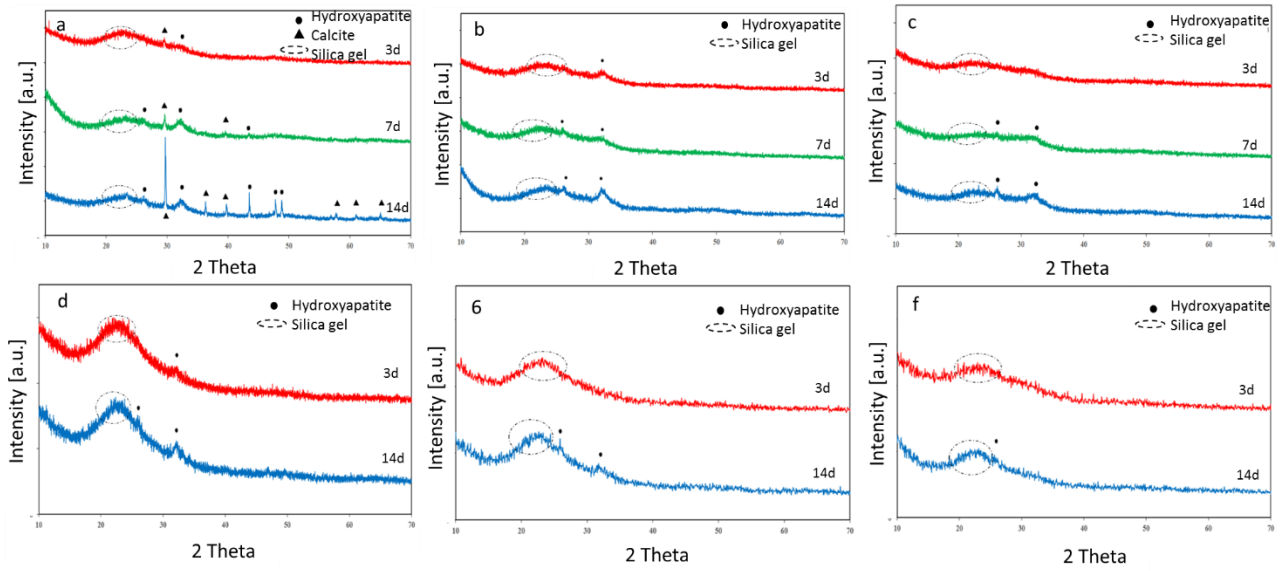

Figure 5: XRD analysis of STe0 (a), STe1 (b) and STe5 (c) powders < 25 μm after 3, 7 and 14 days of SBF treatment, and STe0 (d), STe1 € and STe5 (f) after 3 and 14 days of TRIS treatment.

The glasses reactivity was also investigated using FT-IR (Figure 6) and Raman (Figure 7) analysis. FT-IR measurements evidenced a clear change in the glass spectra after SBF and TRIS immersion. In particular, after SBF treatment (Figure 6a-c) the δ(Si-O-Si) band at about 800 cm^{-1} appeared and the characteristic band of SiO_{NBO} significantly decrease and shift to high wavelength; the broad peak at about 1040 cm^{-1} can be assigned to the stretching PO_4 vibration and the shoulder at 1230 cm^{-1} is ascribable to the formation of new Si-O-Si bonds due to the SiOH condensation [39, 40]. The HAp formation on glass surfaces is confirmed by the presence of a small peak at about 870 cm^{-1}, ascribable to the CO_3^{2-} group in carbonated apatite, and by the appearance of a double peak at 1430 and 1500 cm^{-1} attributed both to Ca^{2+} coordinated CO_3^{2-} adsorption or carbonate ions substituted in carbonated apatite [41, 48, 49]. As already noticed in the XRD analysis, the bands characteristic for HAp are more intense for STe0 glass. Moreover, a small peak at about 710 cm^{-1}, which can be attributed to calcite, was observed for STe0 glass and the band associated with the Te-O at about 700 cm^{-1} decreases during SBF immersion.

The spectra related to the glasses soaked in TRIS solution (Figure 6d-f) evidenced again the bands related to δ(Si-O-Si), SiO_{NBO}, PO_4 vibration and Si-O-Si bonds at 800, 950, 1040 and 1230 cm^{-1} respectively; while the bands ascribable to HAp formation at 870, 1430 and 1500 cm^{-1} are less intense, especially for Te-doped glasses, confirming the lower precipitation rate observed by means of XRD analysis.

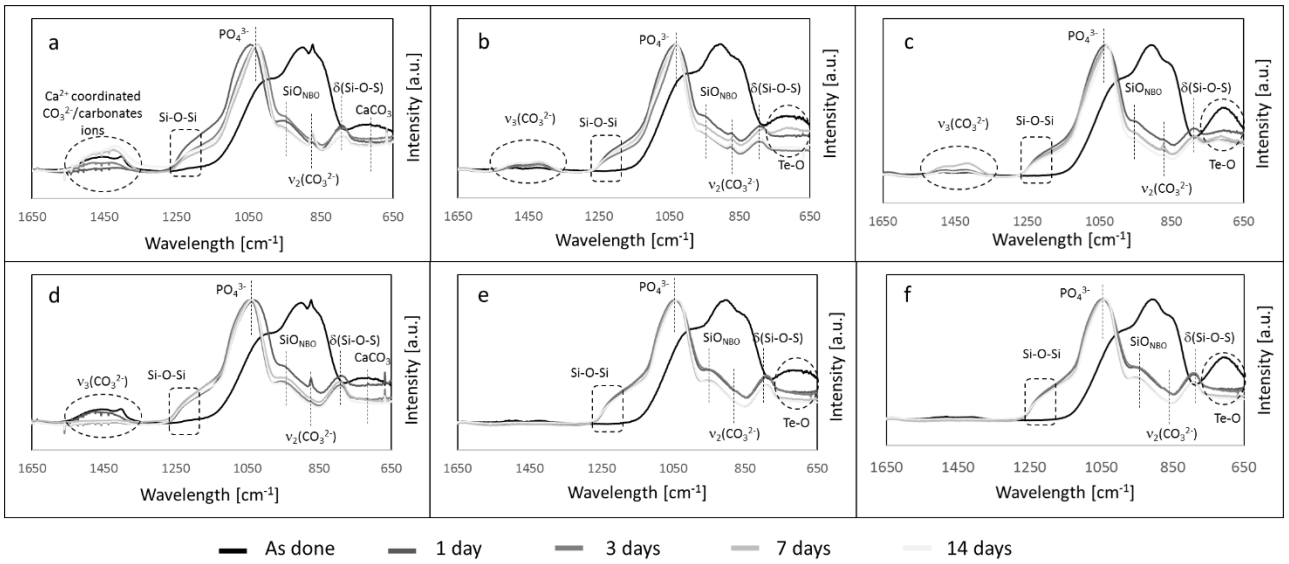

Figure 6: FT-IR analysis of STe0 (a), STe1 (b) and STe5 (c) powders < 25 μm as done and after SBF soaking, and STe0 (d), STe1 (e) and STe5 (f) as done and after TRIS treatment.

Figure 7 shows the Raman spectra of glasses soaked in SBF and TRIS for 14 days and for comparison the graphs of as produced glasses. The spectra of pure glasses evidenced the presence of a band between 350-500 cm^{-1} that can be associated to siliceous bulk vibrational modes, a peak at about 635 cm^{-1} due to the Si-O-Si group, a peak around 860 cm^{-1} and a band between 900-1150 cm^{-1} ascribable to the Si-O-Si bond in silica tetrahedra with a different number of NBO, together with a signal at about 950 cm^{-1} attributed to PO_4 groups [47, 50]. Moreover, the broad peak centered at about 770 cm^{-1} observed in Te-containing glasses is associated to the stretching vibrations of [TeO_4] and [TeO_3] structural units [51].

After soaking in SBF (Figure 7a-c) and TRIS (Figure 7d-f) a new peak appeared at 430 cm^{-1}, which can be y assigned to a crystalline HAp-like structure [50]; in addition, the peak attributable to PO_4 group shifted to 960 cm^{-1} and became sharper [47, 50]. Finally, a more defined peak is observable at 1070 cm^{-1} and can be associated to carbonate groups in carbonated-HAp [47].

Also in this case, a slight delay in HAp nucleation was observed for STe5 glass and the features characteristics of HAp are more intense in the spectra obtained after SBF treatment than TRIS soaking.

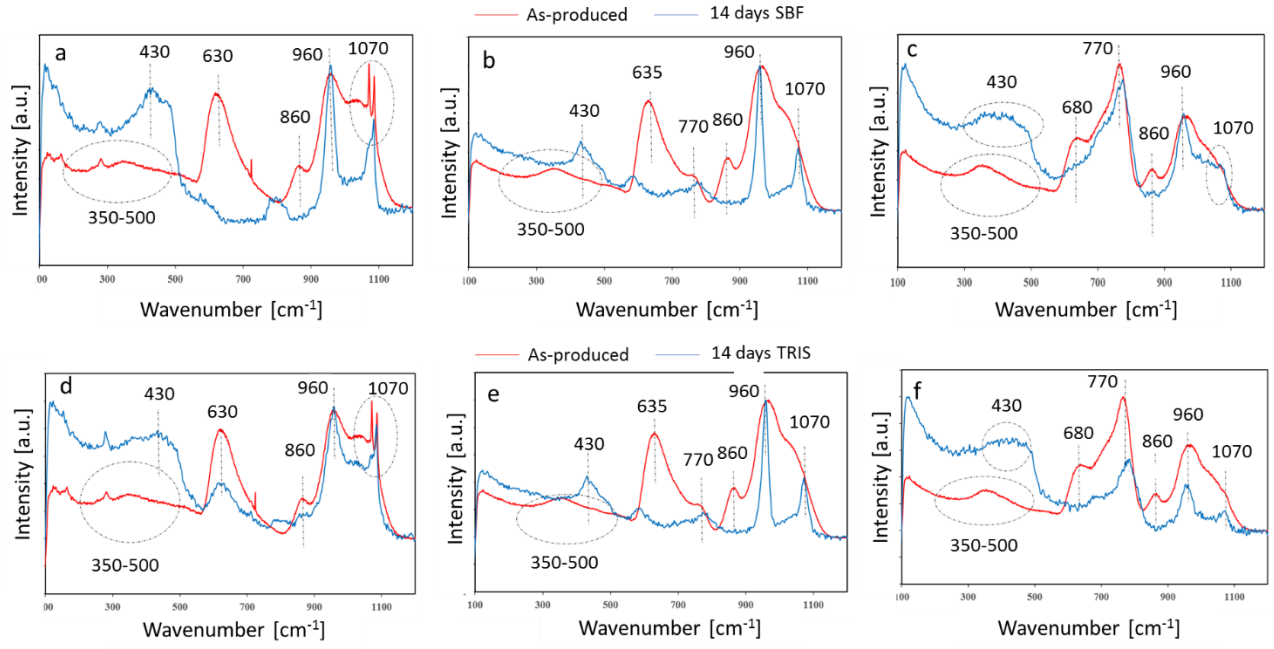

Figure 7: Raman analysis of STe0 (a,d), STe1 (b,e) and STe5 (c,f) powders < 25 μm as-prepared after SBF (a-c) and TRIS (d-f) soaking for 14 days.

The pH trend of STe0, STe1 and Ste5 after immersion in SBF solution was very similar; for all glasses the pH started to increase after the immersion, reached the maximum value (about 8.25) after 1 day and then stabilized. After the glasses immersion in TRIS solution, the pH started to increase and reached the maximum values (7.9-8.1) after 3-7 days. In this case, the STe0 trend reached values slightly lower than Te-containing glasses for the whole immersion time.

3.3 *Biological characterizations*

3.*3.1 Cytocompatibility and ROS/RNS scavenge ability*

Bioactive glasses are a well-known and established category of biomaterials aimed at bone replacement and repair due to their ability to promote the naïve bone healing [5, 52, 53]. In fact, the osteoinductive and osteoconductive properties of bioactive glasses are attributable to the continuous Ca^{2+} and Na^{+} ions release that leads to the formation of a hydrated silica gel layer on the surface that is fast crystallized into a hydroxycarbonate apatite layer [5, 52, 53]. Moreover, many ions such as silver [18, 54], copper [9, 12, 55], strontium [56] and magnesium [57] have been investigated to impart a therapeutic activity to the bioactive glasses; however, to the best of our knowledge this is the first time that tellurium was used as doping element in a bioactive glass composition to obtain a osteogenic, anti-bacterial and anti-inflammatory material. Accordingly, a first *in vitro* specimens' cytocompatibility evaluation was done towards mesenchymal stem cells that were selected as representative cells deputed to undertake the self-healing process [58]. Results are summarized in figure 8a. In general, tellurium doping did not increase bioactive glass specimens' toxicity; in fact, results obtained from cells metabolic activity assay were comparable between tellurium-doped specimens (STe1 and STe5) and untreated controls (STe0, $p>0.05$) within a 72 hours long test period. As prior mentioned, it is not easy to compare these findings with previous literature as tellurium was never applied to bioactive glasses or cements or other bone-dedicated materials as well as only few works deal with the cytocompatibility of tellurium for biomedical applications. However, in those few examples tellurium was describes as a safe element: Lu et al. showed that a tellurium-based antioxidant was effective in modulating H_2O_2-induced inflammation and thus to preserve the viability and the ALP release of MC3T3 pre-osteoblasts from oxidative stress without any side toxic effect [59]. Similarly, Vernet Crua et al. demonstrated that tellurium nanowires hold a targeted toxic effect towards cancerous melanoma cells while no side effects were noticed when the same materials were applied in contact with healthy dermal fibroblasts [60].

However, despite these promising results, much more information are still required to better understand the safety rage of tellurium; here, we can hypothesize that it is not toxic within a 5% molar range when combined with bioactive glasses.

Unlike cytocompatibility, tellurium anti-inflammatory properties have been clearly proved. From this point of view some very promising examples are reported in literature: Dardik et al. demonstrated that a small organotellurium compound octa-O-bis-(R,R)-tartarate ditellurane was effective in suppresses inflammation in human retinal pigment epithelium [61], while Brodsky et al. showed how the use of tellurium was useful for macrophages modulation through the nitric oxide and NFkappaB signaling [62]. Very promising results were also obtained *in vivo* where tellurium compound AS101 was effective in reducing autoimmune encephalomyelitis by suppress monocyte and T cells infiltration into the central nervous system in mice [63]. Here we evaluated tellurium doping anti-inflammatory efficacy in terms of cells viability preservation [64] under oxidative stress conditions induced by a toxic H_2O_2 dosage (300 μM) [65]. Results are summarized in figure 8b-d. In general, tellurium insertion was effective in protecting cells from apoptosis induced by the H_2O_2 treatment. In fact, while in the untreated controls STe0 specimens' cells viability was significantly reduced after the H_2O_2 treatment after 48 and 72 hours ($p<0.05$, indicated by *), the tellurium doped ones (STe1-STe5) preserved cells metabolic activity as no significant differences were obtained by comparing untreated (not treat) and stressed specimens (+ H_2O_2). So, our results seem to be in line with the previous literature thus confirming cells-protective anti-inflammatory ability of tellurium even when used as a doping for bioactive glasses within a 1-5% molar range.

The correlation between tellurium, cells metabolism and oxidative stress has been confirmed by the supernatants active species (ROS/RNS) scavenge results that are reported in Table 3. In general, obtained values demonstrated that the lack of tellurium (Ste0) determined the highest values of ROS/RNS in comparison with doped ones (STe1 and STe5) at all the time-points without the oxidative stress induced by the H_2O_2. In fact, STe0 ranged from 2045 to 2198 RFU while STe1 from 1700 to 1931 and STe5 from 1606 to 1732, thus showing differences even at the basal level. When the H_2O_2 was added to introduce oxidative stress, a similar trend was observed: STe0 reported the highest values included from 2528 to 2735 RFU while STe1 from 2391 to 2613 and STe5 from 2387 to 2499. Accordingly, we can hypothesize that the hBMSCs viability (Figure 8b-d) was not significantly decreased by the H_2O_2 stress due to the ability of tellurium to restrain the formation of toxic oxygen and nitrogen active species. So, we here confirmed the previous debated tellurium anti-inflammatory properties even when it was embedded into bioactive glasses.

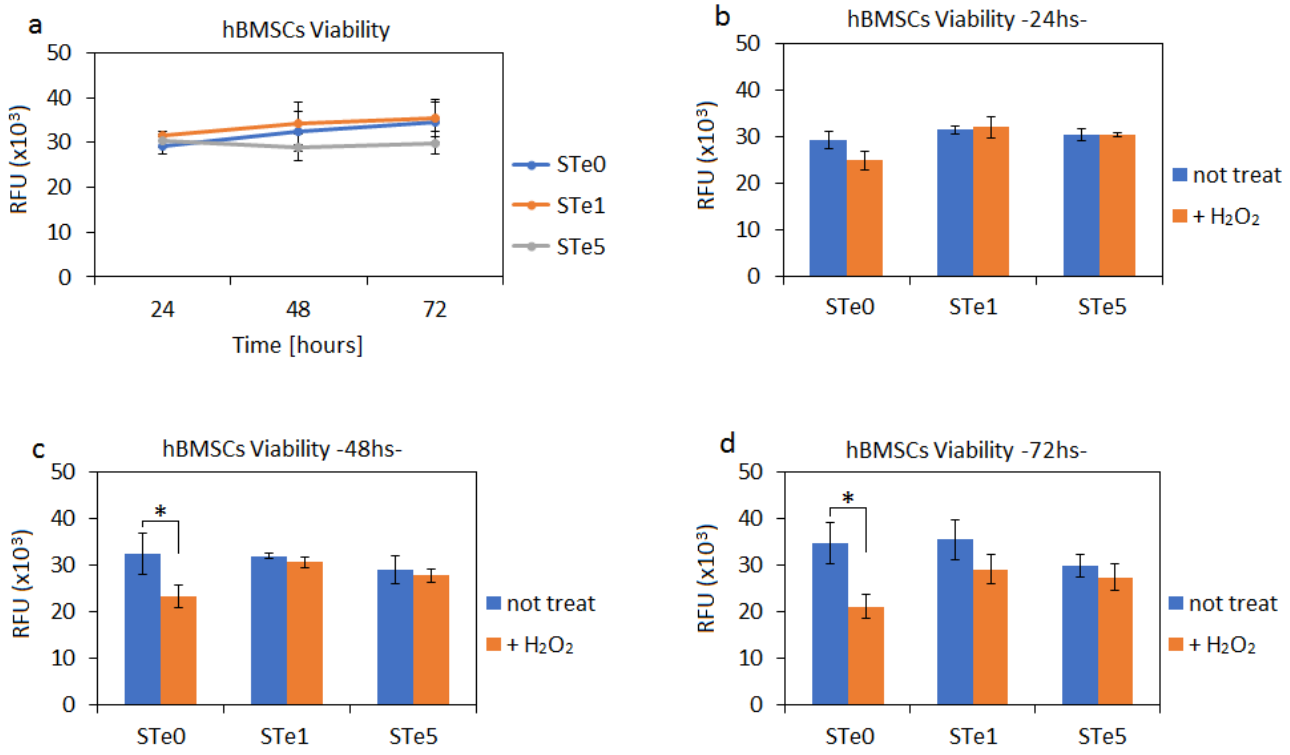

Figure 8. (a) hBMSCs metabolic activity after 24, 48 and 72 hours direct cultivation onto specimens' surface. Tellurium doping (STe1-STe5) did not introduced toxic effects as the metabolism of cells cultivated onto doped specimens was comparable to that obtained onto control ones (STe0, $p>0.05$). (b-d) hBMSCs metabolic activity after 24 (b), 48 (c) and 72 (d) hours direct cultivation onto specimens' surface with (+ H_2O_2) and without (not treat) hydrogen peroxide treatment. While in the untreated controls STe0 specimens' cells viability was significantly reduced after 48 and 72 hours H_2O_2 treatment ($p<0.05$, indicated by *), the tellurium doped ones (STe1-STe5) preserved cells metabolic activity.

Specimen	*Time point (hours)*	*H_2O_2*	*ROS/RNS (RFU)*
STe0	24	-	2045.3 (±25.0)
STeO+H_2O_2	24	+	2528.6 (±44.4)
STe1	24	-	1700.3 (±136.8)
Ste1+ H_2O_2	24	+	2391.6 (±59.6)
STe5	24	-	1606.6 (±76.5)
STe5+ H_2O_2	24	+	2387.6 (±121.0)
STe0	48	-	1975.6 (±96.7)
STeO+ H_2O_2	48	+	2677.0 (±7.5)
STe1	48	-	1723.0 (±99.4)
STe1+ H_2O_2	48	+	2588.6 (±194.9)
STe5	48	-	1547.3 (±27.6)
STe5+ H_2O_2	48	+	2462.6 (±123.0)
STe0	72	-	2198.0 (±223.9)
STeO+ H_2O_2	72	+	2735.0 (±75.1)
STe1	72	-	1931.0 (±42.2)
STe1+ H_2O_2	72	+	2613.0 (±242.0)
STe5	72	-	1732.6 (±48.3)
STe5+ H_2O_2	72	+	2499.0 (±245.4)

Table 3. Supernatant released ROS/RNS quantification (expressed as means ± standard deviation in relative fluorescent units - RFU).

3.3.2 Antibacterial activity

Unlike the lack of a large literature regarding tellurium and tellurium-doped composites cytocompatibility, its antibacterial properties have been demonstrated from many years. Moreover, the antibacterial effect ascribed to the tellurium seem to be broad range and effective towards both planktonic and biofilm species. Zonaro et al. demonstrated that the use of Te^0-based nanoparticles bio-synthesized from tellurite by *Stenotrophomonas maltophilia* and *Ochrobactrum* were effective in decreasing the viability of *Escherichia coli*, *Pseudomonas aeruginosa* and *Staphylococcus aureus* planktonic cells as well as to eradicate the biofilm counterpart [66]. Similarly, Chua et al. identified in the secondary messenger cyclic di-GMP of *Pseudomonas aeruginosa* the pathway affected by tellurite in planktonic and biofilm viability reduction [67].

Tellurium resulted as successful in introducing antibacterial properties even when used as doping element into polymeric composites: a 4% wt tellurium-doped poly(methyl methacrylate) fibers resulted as resistant to *Escherichia coli* K12 strain infection as demonstrated by the CFU count [68].

In this work we decided to test tellurium-doped bioactive glasses towards *Staphylococcus aureus* and *Staphylococcus epidermidis* biofilm because they are the most frequent strains involved in orthopedics infections [69]. Results are summarized in figure 9. The tellurium insertion bestowed to glass a strong ability to inhibit biofilm formation, even if in a dose-dependent manner. In fact, STe1 and STe5 resulted as significant in terms of biofilm metabolic reduction in comparison with the untreated STe0 (considered as control) for both *S. aureus* (Figure 9a, $p<0.05$, indicated by *) and *S. epidermidis* (Figure 9b, $p<0.05$, indicated by *). However, the effect was dose-dependent as STe5 was significant in comparison with STe1 after 48 and 72 hours (Figure 9a-b, $p<0.05$ indicated by the §). Tellurium antibacterial effect is due to a combination of different mechanisms that are probably not yet fully revealed; however, a clear explanation of some of the correlated events were given by Turner et al. [70] and it is schematized in the cartoon in figure 9c. Briefly,

tellurite can exceed the outer membrane as a response to an environmental pH variation and then the toxic metalloid can reach the cytosolic space by exploiting the acetate permease (ActP) transport mechanism. Here, tellurite can be toxic as it is by influencing the activity of the superoxide dismutase (SOD) that is required to counteract the oxygen species (ROS) formed due to the parallel Fenton's reaction involving the metalloid reduction. The same reduction into metallic Te^0 (for example by means of membrane-bound nitrate reductase NAR or thioredoxin-glutathione GSH system) can be toxic due to the accumulation that brings into homeostasis impairment. Based on these considerations, our results seem to be in line with the present literature thus opening to the use of tellurium as an interesting antibacterial tool to improve the resistance towards a possible infection of bioactive glasses.

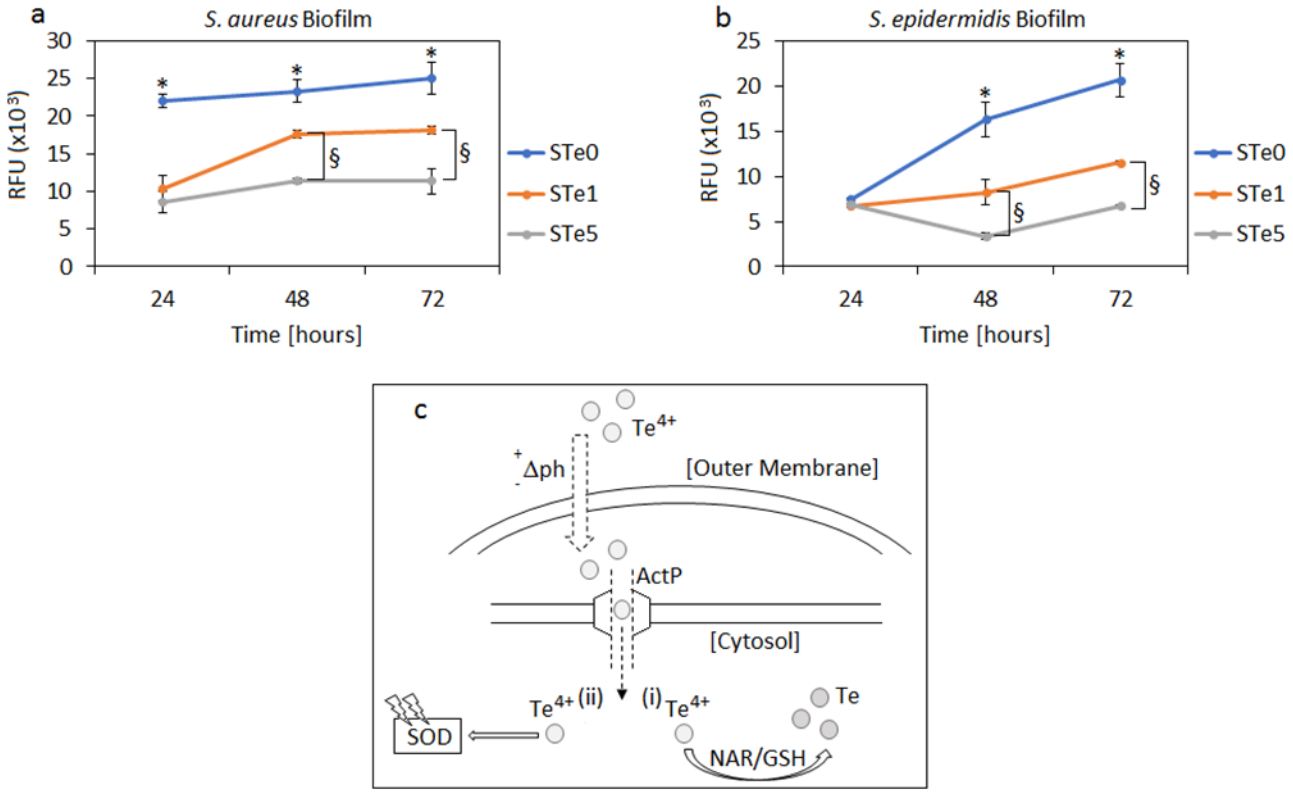

Figure 9. (a) *S. aureus* biofilm metabolic activity evaluation. Tellurium insertion (STe1 and STe5) determined a significant reduction of bacteria viability at time-point in comparison with untreated control STe0 ($p<0.05$, indicated by the *). However, the effect was dose-dependent as STe5 was significant in comparison with STe1 after 48 and 72 hours ($p<0.05$ indicated by the §). (b) *S. epidermidis* biofilm metabolic activity evaluation. Tellurium insertion (STe1 and STe5) determined a significant reduction of bacteria viability in comparison with untreated control STe0 ($p<0.05$, indicated by the Again, a dose-dependent effect was observed as STe5 was significant in comparison with Ste1 after 48 and 72 hours ($p<0.05$ indicated by the §). (c) Schematic representation of tellurium-derived toxicity in bacteria.

3.3.3 Osteogenesis

As prior mentioned, bioactive glasses are materials mainly aimed at bone replacement and healing. Accordingly, here mesenchymal stem cells osteogenic differentiation was considered to study any eventual positive or negative event due to the presence of tellurium. Therefore, the activity of alkaline phosphatase (ALP) was considered over a 7-10-15-21 days period as an indicator of the progressive cell commitment. However, results did not reveal any significant differences in terms of ALP activity by comparing controls (STe0) and tellurium-doped specimens (STe1 and STe5) thus not suggesting any improvement or worsening due to the presence of the metalloid (Figure 10 a, $p>0.05$). These findings are like those previously presented by Lu et al. where the ALP activity of murine pre-osteoblasts MC3T3 cells was not affected after the exposure

to a tellurium-based antioxidant compound [65]. However, very few works directly correlate tellurium and osteogenesis thus making necessary further study to fully evaluate this process.

Afterwards, keeping in mind the promising results obtained by the ROS/RNS scavenge activity, the ALP activity was further evaluated in the presence of H_2O_2-induced oxidative stress. Results are reported in figure 10 b. After 7 and 10 days, no significant differences were noticed between control (STe0) and tellurium-doped ones (STe1 and STe5) and ALP values were comparable to the previous assay performed in the absence of hydrogen peroxide (Figure 10a). However, after 15 and 21 days some differences were noted as STe1 and STe5 ALP results were significant towards STe0 controls (Figure 10b, $p<0.05$, indicated by *) and comparable with the previous H_2O_2-free assay. A direct correlation between tellurium ROS scavenge activity and ALP activity preservation can be hypothesized because H_2O_2 is known to be effective in interfere with osteogenic differentiation including ALP and collagen type I expression by the ERK and ERK-dependent NF-kB activation [71]. Finally, to further prove the mesenchymal stem cells seeded onto STe1 and STe5 specimens were correctly committed towards osteoblast lineage despite the oxidative stress induced by hydrogen peroxide, an alizarin red assay was performed to verify the presence of a bone-like mature calcified matrix. As prior showed by the ALP activity evaluation, alizarin staining conformed that only untreated STe0 specimens significantly decreased the amount of calcified deposits by comparing results with and without H_2O_2 (Figure 10c, $p<0.05$, indicated by the *). On the opposite, alizarin results for STe1 and STe5 were comparable between treated and control groups. So, the tellurium activity in terms of ROS scavenge was effective in preserving osteogenesis of cells cultivated on the surface of bioactive glasses imposed to an oxidative stress condition.

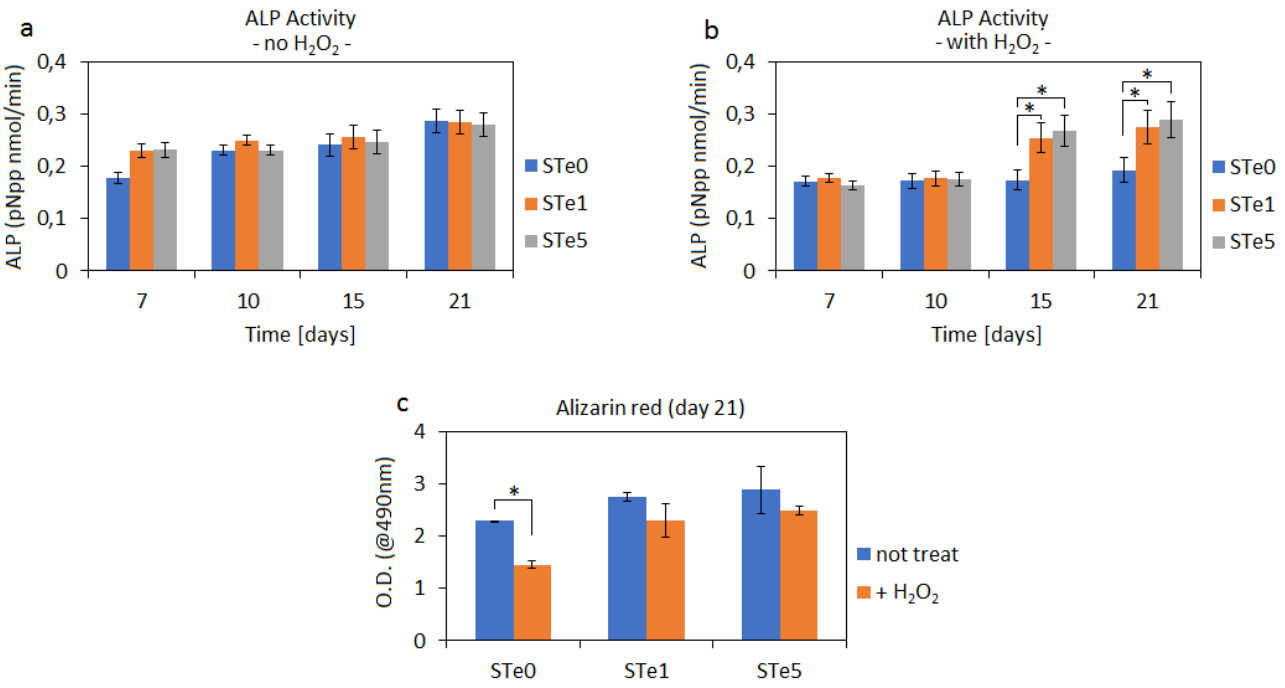

Figure 10: Alkaline Phosphatase and Alizarin red specific osteogenic markers evaluation. Tellurium doping (STe1 and STe5) did not increase ALP activity (a, $p>0.05$) but preserved its expression in presence of pro-inflammatory H_2O_2 (b, $p<0.05$ vs STe0 control, indicated by *). As a confirmation, the amount of calcium deposit evaluated by alizarin red was preserved for STe1 and STe5 while was significantly reduced for STe0 control (c, $p<0.05$, indicated by *).

3.3.4 Cells-bacteria Co-cultures

Further biological tests (co–cultures) were applied in order to evaluate how the doped surfaces can act with respect to the competition between cells and bacteria for surface colonization in a sort of "race for the surface" as firstly postulated by Gristina in 1987 [72]. This assay was designed to resemble the most frequent clinical scenario where patients that underwent orthopedic surgery and bone implantation are subjected to postoperative infection during the late healing. Secondary infections are nowadays more and more frequent thus representing a huge problem for patients due to the need of a second surgery necessary to recover the device fixation [73]. Accordingly, here we first seeded the cells directly onto the specimens' surface and after 24 hours cultivation the infection was induced by inoculating *S. aureus* or *S. epidermidis* as schematized in figure 11 a. Similar procedures were previously applied in literature to evaluate materials' surface properties in order to favor the device colonization from cells over bacteria [74-76]. Our results were very promising from this point of view but unlike antibacterial assays (Figure 9), only STe5 specimens were effective in significantly reduce bacteria number and preserve cells viability when they were cultivated in the same environment (Figure 11 b-e). In fact, when the infection was done with *S. aureus*, the number of viable cells was significantly higher for STe5 in comparison with untreated STe0 (Figure 11b, $p<0.05$, indicated by *) while STe1 was not significant towards control. Similarly, the CFU count reported a significant decrease of viable bacterial colonies only when they were cultivated onto STe5 surfaces (Figure11d, $p<0.05$, indicated by *). The difference between STe1 and STe5 was more evident by using *S. epidermidis* as both viable cells (Figure 11c) and CFU count (Figure 11e) revealed significant results by comparing STe5 vs Ste0 ($p<0.05$, indicated by *) and STe5 vs STe1 ($p<0.05$, indicated by #). Accordingly, only specimens STe5 were effective in preventing infections by the co-culture assays.

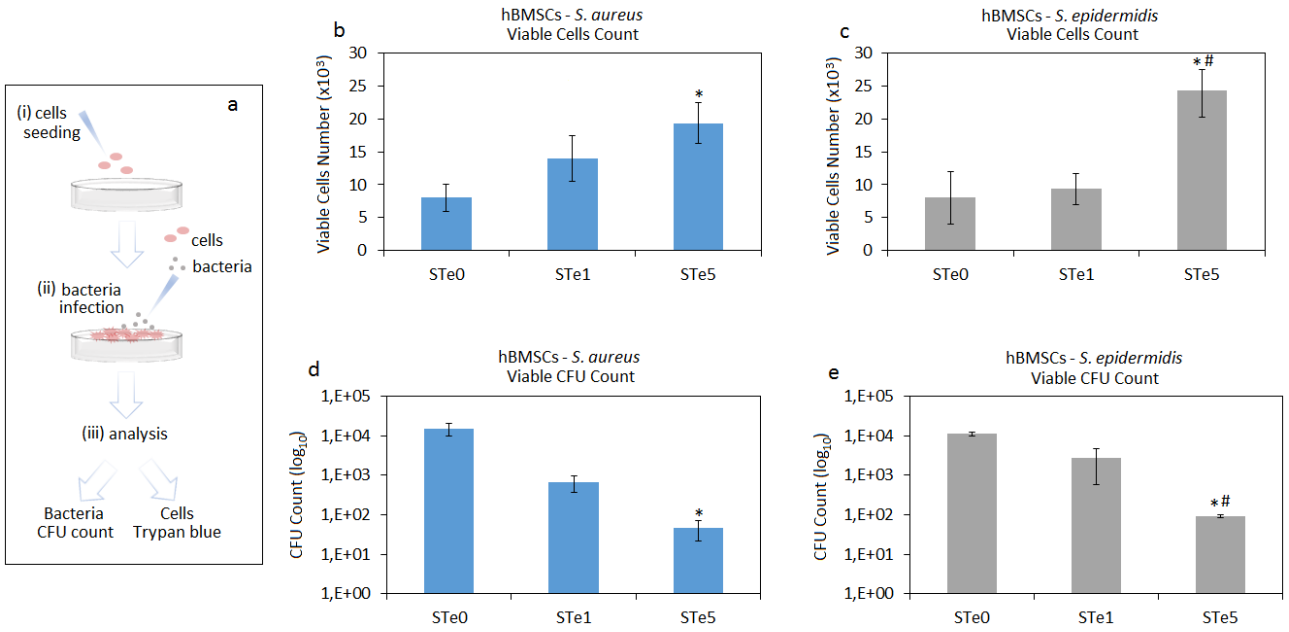

Figure 11: Cells-bacteria co-culture assay. (a) Specimens were pre-seeded with cells and then infected using *S. aureus* (b-d) or *S. epidermidis* (c-e). Results showed that only STe5 were able to significantly preserve cells from the infection in comparison with STe0 (b and c, $p<0.05$, indicated by the *) and STe1 (c, $p<0.05$, indicated by the #); similarly, the CFU number was significantly decreased by STe5 in comparison with STe0 (b and c, $p<0.05$, indicated by the *) and STe1 (c, $p<0.05$, indicated by the #). Bars represent means and standard deviations.

4. Conclusions

In this work Te-doped glasses were synthesized by melt and quenching process and characterized to investigate the influence of Te introduction in the glass properties and the possible biological effect imparted

by Te presence. The performed analyses evidenced that Te-containing glasses showed an amorphous structure and a slight change in characteristic temperature, in particular for glass doped with 5 mol% of TeO_2. The prepared glasses maintained a good degree of bioactivity since they are able to promote the *in vitro* precipitation of HAp in few days.

The biological characterization demonstrated that Te-doped glasses preserved the cytocompatibility; moreover, tellurium insertion was effective in protecting cells metabolic activity from apoptosis induced by the H_2O_2 treatment. Antibacterial test evidenced a clear antibacterial effect of Te-containing glasses and a strong ability to inhibit biofilm formation, in a dose-dependent manner. The evaluation of osteogenic markers confirmed the ability of Te-containing glasses to preserve the ALP and Alizarin red expression in presence of an oxidative stress. Finally, cells-bacteria co-cultures confirmed that Te presence significantly preserve cells from the infection, in particular for STe5 glass.

Therefore, thanks to the strong antibacterial and antioxidant properties as well as the cytocompatibility here demonstrated, tellurium appears as a novel and interesting element to improve the biological properties of bioactive glasses specially for the treatment of complicated cases such as infected and inflamed bone fractures.

References

[1] L.L. Hench, Bioceramics, J. Am. Ceram. Soc. 81 (1993) 705–1728.

[2] W. Cao, L.L. Hench, Bioactive materials, Ceram. Int. 22 (1996) 493–507.

[3] V. Miguez-Pacheco, L.L. Hench, A.R. Boccaccini, Bioactive glasses beyond bone and teeth: Emerging applications in contact with soft tissues, Acta Biomat. 13 (2015) 1-15.

[4] V. Miguez-Pacheco, D. Greenspan, L.L. Hench, A.R. Boccaccini, Bioactive glasses in soft tissue repair, Am. Cer. Soc. Bull. 94 (2015) 27-31.

[5] F.Baino, S. Hamzehlou, S. Kargozar, Bioactive Glasses: Where Are We and Where Are We Going? J Funct Biomater. 9(1) (2018) 25.

[6] J. Isaac, J. Nohra, J. Lao, E. Jallot, J.M. Nedelec, A. Berdal, J.M.Sautier, Effects of strontium-doped bioactive glass on the differentiation of cultured osteogenic cells, Eur. Cell Mater. 21 (2011) 130-143.

[7] E. Verné, S. Di Nunzio, M. Bosetti, P. Appendino, C. Vitale Brovarone, G. Maina, M. Cannas, Surface characterization of silver-doped bioactive glass, Biomaterials. 26 (2005) 5111–5119.

[8] M. Mozafari, F. Moztarzadeh, F. Moztarzadeh, Silver-doped Bioactive Glasses: What Remains Unanswered? InterCeram: International Ceramic Review 62(6) (2013) 423-425

[9] M. Miola, E. Verné, Bioactive and Antibacterial Glass Powders Doped with Copper by Ion-Exchange in Aqueous Solutions, Materials 9(6) (2016) 405.

[10] L.B. Romero-Sánchez, M. Marí-Beffa, P. Carrillo, M.Á. Medina, A. Díaz-Cuenca, Copper-containing mesoporous bioactive glass promotes angiogenesis in an in vivo zebrafish model, Acta Biomater. 68 (2018) 272-285.

[11] M. Miola, C. Vitale Brovarone, G. Maina, F. Rossi, L. Bergandi, D. Ghigo, S. Saracino, M. Maggiora, R.A. Canuto, G. Muzio, E. Vernè, In vitro study of manganese-doped bioactive glasses for bone regeneration, Mater. Sci. Eng. C. 38 (2014) 107–118.

[12] K. Zheng, X. Dai, M. Lu, N. Hüser, N. Taccardi, A.R.Boccaccini, Synthesis of copper-containing bioactive glass nanoparticles using a modified Stöber method for biomedical applications, Colloids Surf B Biointerfaces. 150 (2017) 159-167.

[13] V. Mourino, J.P. Cattalini, A.R. Boccaccini, Metallic ions as therapeutic agents in tissue engineering scaffolds: an overview of their biological applications and strategies for new developments, J. R. Soc. Interface 9 (2012) 401–419.

[14] L.L. Hench, Genetic design of bioactive glass, J. Eur. Ceram. Soc. 29 (7) (2009) 1257–1265.

[15] A. Hoppe, N.S. Güldal, A.R. Boccaccini, A review of the biological response to ionic dissolution products from bioactive glasses and glass-ceramics, Biomat. 32 (2011) 2757-2774.

[16] A. Hoppe, V. Mouriño, A.R. Boccaccini, Therapeutic inorganic ions in bioactive glasses to enhance bone formation and beyond. Biomater, Sci., 1 (2013) 254-256.

[17] R.H. Fernandes, A. Gaddam, A. Rebelo, D. Brazete, G.E. Stan, J.M.F. Ferreira, Bioactive Glasses and Glass-Ceramics for Healthcare Applications in Bone Regeneration and Tissue Engineering Materials (Basel), 11(12) (2018) 2530.

[18] E. Verné, M. Miola, C. Vitale Brovarone, M. Cannas, S. Gatti, G. Fucale, G. Maina, A. Massé, S. Di Nunzio, Surface silver-doping of biocompatible glass to induce antibacterial properties. Part I: massive glass. J. Mat. Sci. Mat. Med, Vol. 20(3) (2009) 733-7440.

[19] H. Palza, B. Escobar, J. Bejarano,D. Bravo, M. Diaz-Dosque, J. Perez. Designing antimicrobial bioactive glass materials with embedded metal ions synthesized by the sol-gel method. 33(7) (2013) 3795-3801.

[20] S. Kaya, M. Cresswell, A.R. Boccaccini, Mesoporous silica-based bioactive glasses for antibiotic-free antibacterial applications, Mat.Sci. Eng.: C 83 (2018) 99-107.

[21] A. Pedone, F. Muniz-Miranda, A. Tilocca, M.C. Menziani, The antioxidant properties of Ce-containing bioactive glass nanoparticles explained by Molecular Dynamics simulations, 2 (2016) 19-28.

[22] B. Aslam, W. Wang, M.I. Arshad, M. Khurshid, S. Muzammil, M.H. Rasool, M.A. Nisar, R.F. Alvi, M.A. Aslam, M.U. Qamar, M.K.F. Salamat, Z. Baloch, Antibiotic resistance: a rundown of a global crisis, Infect Drug Resist. 11 (2018) 1645-1658.

[23] J.L. Hobman, L.C. Crossman, Bacterial antimicrobial metal ion resistance. J. Med. Microb. 64 (2014) 471–497.

[24] J.Y. Maillard, P. Hartemann. Silver as an antimicrobial: Facts and gaps in knowledge. Crit Rev Microbiol. 39(4) (2013) 373-383.

[25] L.A. Ba, M. D¨oring, V. Jamier, C. Jacob, Tellurium: an element with great biological potency and potential Org. Biomol. Chem., 8 (2010) 4203–4216.

[26] Z. Cailing, Q. Biyin, X. Xinyuan, B. Yan, Antioxidant and Antimicrobial Activity of Tellurium Dioxide Nanoparticles Sols, J. Nano Res. Online: 25 (2013) 8-15.

[27] M. Shakibaie, M. Adeli-Sardou, T. Mohammadi-Khorsand, M. Zeydabadi- Nejad, E. Amirafzali, S. Amirpour-Rostami, A. Ameri, H. Forootanfar, Antimicrobial and Antioxidant Activity of the Biologically Synthesized Tellurium Nanorods; A Preliminary In vitro Study, Iranian J Biotech. 15(4) (2017) e1580.

[28] M.G. Ma, J.F. Zhu, R.C. Sun, F. Chen, Y.J. Zhu, Synthesis and characterization of the tellurium/calcium silicate nanocomposite, Materials Letters 65 (2011) 424–426.

[29]G. El-Damrawi, H. Doweidar, H. Kamal, Characterization of New Categories of Bioactive Based Tellurite and Silicate Glasses, Silicon, 9, (2017) 503–509.

[30] T. Kokubo, H. Takadama, How useful is SBF in predicting in vivo bone bioactivity? Biomaterials 27 (2006) 2907–2915.

[31]UNI EN ISO 10993-15, Valutazione biologica dei dispositivi medici - Identificazione e quantificazione dei prodotti di degradazione da metalli e leghe, 2002.

[32] A. Macon, T.B. Kim, E.M. Valliant, K. Goetschius, R.K. Brow, D.E. Day, A. Hoppe, A.R. Boccaccini, I.Y. Kim, C. Ohtsuki, T. Kokubo, A. Osaka, M. Vallet-Regı, D.Arcos, L. Fraile, A.J. Salinas, A.V. Teixeira, Y. Vueva, R.M. Almeida, M. Miola, C. Vitale-Brovarone, E. Vernè, W. Ho¨land, J. R. Jones, A unified in vitro evaluation for apatite-forming ability of bioactive glasses and their variants, J. Mater. Sci. Mater. Med., 26 (2015) 115.

[33] S. James, J. Fox, F. Afsari, J. Lee, S. Clough, C. Knight, J. Ashmore, P. Ashton, O. Preham, M. Hoogduijn, R.D.A.R. Ponzoni, Multiparameter analysis of human bone marrow stromal cells identifies distinct immunomodulatory and differentiation-competent subtypes, Stem Cell Reports 4 (2015) 1004- 15.

[34] X. Lu, G. Mestres, V.P. Singh, P. Effati, J.F. Poon, L. Engman, M.K.Ott, Selenium- and Tellurium-Based Antioxidants for Modulating Inflammation and Effects on Osteoblastic Activity, Antioxidants 6(1) (2017) E13.

[35] A. Cochis, B. Azzimonti, C. Della Valle, E. De Giglio, N. Bloise, L. Visai, S. Cometa, L. Rimondini, R. Chiesa, The effect of silver or gallium doped titanium against the multidrug resistant Acinetobacter baumannii, Biomaterials, 80 (2016) 80-95.

[36] S. Ferraris, A. Cochis, M. Cazzola, M. Tortello, A. Scalia, S. Spriano, L. Rimondini, Cytocompatible and Anti-bacterial Adhesion Nanotextured Titanium Oxide Layer on Titanium Surfaces for Dental and Orthopedic Implants, Front Bioeng Biotechnol. 7 (2019) 103.

[37] A. Jekabsone, I. Sile, A. Cochis, M. Makrecka-Kuka, G. Laucaityte, E. Makarova, L. Rimondini, R. Bernotiene, L. Raudone, E. Vedlugaite, R. Baniene, A. Smalinskiene, N. Savickiene, M. Dambrova, Investigation of Antibacterial and Antiinflammatory Activities of Proanthocyanidins from Pelargonium sidoides DC Root Extract, Nutrients. 11(11)(2019) 2829.

[38] J.J. Harrison, C.A. Stremick, R.J. Turner, N.D. Allan, M.E. Olson, H.C eri, Microtiter susceptibility testing of microbes growing on peg lids: a miniaturized biofilm model for highthroughput screening. Nat. Protoc. 5 (2010) 1236–1254.

[39] U. Boonyang, F. Li, A. Stein, Hierarchical Structures and Shaped Particles of Bioactive Glass and Its In Vitro Bioactivity, J. Nanomat. 2013 (2013) 681391.

[40] M. Mačković, A. Hoppe, R. Detsch, D. Mohn, W.J. Stark, E.Spiecker, A.R. Boccaccini, Bioactive glass (type 45S5) nanoparticles: in vitro reactivity on nanoscale and biocompatibility, J Nanoparticle Res, 14 (2012) 96.

[41] M. Cerruti, D. Greenspan, K. Powers, Effect of pH and ionic strength on the reactivity of Bioglass_ 45S5, Biomaterials 26(14) (2005) 1665–1674.

[42] H. Du, C.T. Williams, A.D. Ebner, J.A. Ritter, In situ FTIR spectroscopic analysis of carbonate transformations during adsorption and desorption of CO_2 in K-promoted HTlc. Chem Mater 22(11) (2010) 3519–3526.

[43] G. El-Damrawi, H. Doweidar, H. Kamal, Characterization of New Categories of Bioactive Based Tellurite and Silicate Glasses Silicon 9 (2017) 503–509.

[44] N. Berwal , S. Dhankhar, P. Sharma, R.S. Kundu, R. Punia, N. Kishore, Physical, structural and optical characterization of silicate modified bismuth-borate-tellurite glasses. J. Molecular Structure 1127 (2017) 636-644.

[45] M. F. Faznny, Halimah Mohamed Kamari, Farah Diana Muhammad, Show all 5 authors, Zaitizila Ismail. Structural and Optical Properties of Zinc Borotellurite Glass Co-Doped with Lanthanum and Silver Oxide. J Mat. Sci. Chem. Eng. 06(04) (2018) 18-23.

[46] A.C.M. Rodrigues, R. Keding, C. Rüssel, Mixed former effect between TeO_2 and SiO_2 in the $Li_2O{\cdot}TeO_2{\cdot}SiO_2$ system,j. Non-Cryst. Sol. 273 (2000) 53-58.

[47] D. Bellucci, G. Bolelli, V. Cannillo, A. Cattini, In situRaman spectroscopy investigation of bioactive glass reactivity: Simulated body fluid solution vs TRIS-buffered solution, Mat. Characteriz. 62 (2011) 1021-1028.

[48] S. Koutsopoulos, Synthesis and characterization of hydroxyapatite crystals: A review study on the analytical methods, J Biomed Mater Res 62(4) (2002) 600-612.

[49] I. Notingher, J. R. Jones, S. Verrier, I. Bisson, P. Embanga, P. Edwards, J. M. Polak, L. L. Hench, Application of FTIR and Raman Spectroscopy to Characterisation of Bioactive Materials and Living Cells. Spectroscopy 17 (2003) 275-288.

[50] F. Bonino, A. Damin, V. Aina, M. Miola, E. Verne, O. Bretcanu, S. Bordiga, A. Zecchina, C. Morterra, In situ Raman study to monitor bioactive glasses reactivity. J. Raman Spectrosc. 39 (2008) 260–264.

[51] Swapna, G. Upender, M. Prasad, Raman, FTIR, thermal and optical properties of TeO2-Nb2O5-B2O3-V2O5 quaternary glass system, J.Taibah Univ. for Sci. 11 (2017) 583-592.

[52] G. Kaur, G. Pickrell, N. Sriranganathan, V. Kumar, D. Homa, Review and the state of the art: Sol–gel and melt quenched bioactive glasses for tissue engineering. J. Biomed. Mater. Res. Part B 104B (2016) 1248–1275.

[53] M. Karadjian, C. Essers, S. Tsitlakidis, B. Reible, A. Moghaddam, A.R. Boccaccini, F. Westhauser, Biological Properties of Calcium Phosphate Bioactive Glass Composite Bone Substitutes: Current Experimental Evidence. Int J Mol Sci. 20(2) 2019 E305.

[54] P.J. Newby, R. El-Gendy, J. Kirkham, X.B. Yang, I.D. Thompson, A.R. Boccaccini, Ag-doped 45S5 Bioglass®-based bone sca_olds by molten salt ion exchange: Processing and characterisation. J. Mater. Sci. Mater. Med. 22 (2011) 557–569.

[55] M. Miola, A. Cochis, A. Kumar, C.R. Arciola, L. Rimondini, E. Verné, Copper-Doped Bioactive Glass as Filler for PMMA-Based Bone Cements: Morphological, Mechanical, Reactivity, and Preliminary Antibacterial Characterization. Materials 11(6) (2018) E961.

[56] A.C. Özarslan, S. Yücel Fabrication and characterization of strontium incorporated 3-D bioactive glass scaffolds for bone tissue from biosilica. Mater Sci Eng C Mater Biol Appl. 68 (2016) 350-357.

[57] D. Bellucci, A. Sola, R. Salvatori, A. Anesi, L. Chiarini, V. Cannillo, Role of magnesium oxide and strontium oxide as modifiers in silicate-based bioactive glasses: Effects on thermal behaviour, mechanical properties and in-vitro bioactivity, Mater Sci Eng C Mater Biol Appl. 72 (2017) 566-575.

[58] W. Lin, L. Xu, S. Zwingenberger, E. Gibon, S,B. Goodman, G. Li, Mesenchymal stem cells homing to improve bone healing, J Orthop Translat. 9 (2017) 19-27.

[59] X. Lu, G. Mestres, V.P. Singh, P. Effati, J.F. Poon, L. Engman, M.K. Ott, Selenium- and Tellurium-Based Antioxidants for Modulating Inflammation and Effects on Osteoblastic Activity, Antioxidants 6(1) (2017) E13.

[60] A. Vernet Crua, D. Medina, B. Zhang, M.U. González, Y. Huttel, J.M. García-Martín, J.L. Cholula-Díaz, T.J. Webster, Comparison of cytocompatibility and anticancer properties of traditional and green chemistry-synthesized tellurium nanowires, Int J Nanomedicine. 14 (2019) 3155-3176.

[61] R. Dardik, T. Livnat, G. Halpert, S. Jawad, Y. Nisgav, S. Azar-Avivi, B. Liu, R.B. Nussenblatt, D. Weinberger, B. Sredni, The small tellurium-based compound SAS suppresses inflammation in human retinal pigment epithelium, Mol Vis. 22 (2016) 548-562.

[62] M. Brodsky, G. Halpert, M. Albeck, B. Sredni, The anti-inflammatory effects of the tellurium redox modulating compound, AS101, are associated with regulation of NFkappaB signaling pathway and nitric oxide induction in macrophages, J Inflamm (Lond). 7(1) (2010) 3.

[63] J.H. Lee, M. Halperin-Sheinfeld, D. Baatar, M.R. Mughal, H.J. Tae, J.W. Kim, A. Carter, A. Lustig, O. Snir, G. Lavie, E. Okun, M.P. Mattson, B. Sredni, D.D.Taub, Tellurium compound AS101 ameliorates experimental autoimmune encephalomyelitis by VLA-4 inhibition and suppression of monocyte and T cell infiltration into the CNS, Neuromolecular Med. 16(2) (2014) 292-307.

[64] E. Varini, S. Sánchez-Salcedo, G. Malavasi, G. Lusvardi , M. Vallet-Regí, A.J. Salinas Cerium (III) and (IV) containing mesoporous glasses/alginate beads for bone regeneration: bioactivity, biocompatibility and reactive oxygen species activity. Mater Sci Eng C Mater Biol Appl. 105 (2019) 109971.

[65] X. Lu, G. Mestres, V.P. Singh, P. Effati, J.F. Poon, L. Engman, M.K.Ott Selenium- and Tellurium-Based Antioxidants for Modulating Inflammation and Effects on Osteoblastic Activity, Antioxidants 6(1) (2017) E13.

[66] E. Zonaro, S. Lampis, R.J. Turner, S.J. Qazi, G. Vallini, Biogenic selenium and tellurium nanoparticles synthesized by environmental microbial isolates efficaciously inhibit bacterial planktonic cultures and biofilms. Front Microbiol. 6 (2015) 584.

[67] S.L. Chua, K. Sivakumar, M. Rybtke, M. Yuan, J.B. Andersen, T.E. Nielsen, M. Givskov, T. Tolker-Nielsen, B. Cao, S. Kjelleberg, L. Yang, C-di-GMP regulates Pseudomonas aeruginosa stress response to tellurite during both planktonic and biofilm modes of growth. Sci Rep. 5 (2015) 10052.

[68] R.K. Matharu, Z. Charani, L. Ciric, Illangakoon, U.E., Edirisinghe, M. Antimicrobial activity of tellurium-loaded polymeric fiber meshes. J. Appl. Polym. Sci. 135 (2018) 46368.

[69] R. Sorrentino, A. Cochis, B, Azzimonti, C. Caravaca, J. Chevalier, M. Kuntz, A.A. Porporati, R.M. Streicher, L. Rimondini, Reduced bacterial adhesion on ceramics used for arthroplasty applications. Journal of the Europ. Cer. Soc. 38(3) (2018) 963-970.

[70] R.J. Turner, R. Borghese, D. Zannoni, Microbial processing of tellurium as a tool in biotechnology. Biotechnol Adv. 30(5) (2012) 954-963.

[71] X.C. Bai, D. Lu, J. Bai, H. Zheng, Z.Y. Ke, X.M. Li, S.Q. Luo, Oxidative stress inhibits osteoblastic differentiation of bone cells by ERK and NF-kappaB. Biochem. Biophys, Res. Commun. 314 (2004) 197–207.

[72] A.G. Gristina, Biomaterial-centered infection: microbial adhesion versus tissue integration, Science., 237 (4822) (1987) 1588-1595

[73] X. Zhang, X. Zhan, P. Zou, H. An, Factors related to infection after fixation in the process of late healed bone fracture, Exp Ther Med. 14(2) (2017) 1126-1130.

[74] G. Subbiahdoss, R. Kuijer, D.W. Grijpma, H.C. van der Mei, H.J. Busscher, Microbial biofilm growth vs. Tissue integration: "the race for the surface" experimentally studied, Acta Biomater., 5 (5) (2009) 1399-1404

[75] D.B. McConda, J.M. Karnes, T. Hamza, B.A. Lindsey, A novel co-culture model of murine K12 osteosarcoma cells and S. Aureus on common orthopedic implant materials:' the race to the surface' studied in vitro, Biofouling. 32 (6) (2016) 627-634.

[76] J.H. Lee, H. Wang, J.B. Kaplan, W.Y. Lee, Effects of Staphylococcus epidermidis on osteoblast cell adhesion and viability on a Ti alloy surface in a microfluidic co-culture environment, Acta Biomater., 6 (11) (2010) 4422-4429.